Electron Raman scattering in semiconductor quantum well wire of cylindrical ring geometry

Re. Betancourt-Riera[a)b)†], Ri. Betancourt-Riera[a)], J. M. Nieto Jalil[c)], and R. Riera[b)]

[a)] *Instituto Tecnológico de Hermosillo. Avenida Tecnológico S/N, Col. Sahuaro, C.P.* 83170, *Hermosillo, Sonora, México*
[b)] *Departamento de Investigación en Física, Universidad de Sonora, Apartado Postal* 5-088, *C.P.* 83190, *Hermosillo, Sonora, México*
[c)] *Tecnológico de Monterrey-Campus Sonora Norte. Bulevar Enrique Mazón López No.* 965, *C.P.* 83000, *Hermosillo, Sonora, México*

(Received 11 March 2015; revised manuscript received 11 June 2015; published online 9 October 2015)

We study the electron states and the differential cross section for an electron Raman scattering process in a semiconductor quantum well wire of cylindrical ring geometry. The electron Raman scattering developed here can be used to provide direct information about the electron band structures of these confinement systems. We assume that the system grows in a GaAs/$Al_{0.35}Ga_{0.65}As$ matrix. The system is modeled by considering $T = 0$ K and also a single parabolic conduction band, which is split into a sub-band system due to the confinement. The emission spectra are discussed for different scattering configurations, and the selection rules for the processes are also studied. Singularities in the spectra are found and interpreted.

Keywords: electron states, Raman scattering, selection rules, quantum well wires

PACS: 73.21.Hb, 78.67.Lt **DOI:** 10.1088/1674-1056/24/11/117302

1. Introduction

Owing to the promising physical features, the low-dimensional semiconductor nanostructures have been widely investigated both experimentally and theoretically.[1,2] Because of their potential technological applications, in the last decade, there have been many studies on the semiconductor quantum well wire of cylindrical ring geometry. This system is an excellent candidate for various optoelectronic, high temperature, and high-frequency device applications, such as light-emitting diodes, laser diodes, field-effect transistors, solar cells, chemical and biological sensors.[3] Recently, spin-dependent electron transport in the mesoscopic system has attracted considerable attention because of its potential application in a new scientific area, spintronics, where the spin degree of freedom may be utilized to process information.[4] The experimental research on Raman scattering in nanocrystals has been extensively reported.[5–12] To interpret the experimental results, the theoretical research usually focused on the calculation of the differential cross-section (DCS) for Raman scattering.[13,14] Thus, the calculation of the DCS for electron Raman scattering (ERS) remains a rather interesting and fundamental issue.[15] Recently, the experimental research on the Raman scattering in the GaN semiconductor quantum well wire of cylindrical ring geometry was reported.[16–19]

When studying a physical system from the viewpoint of quantum mechanics, the properties of the physical system are contained in the system wave function. In this work, we determine the stationary states of an electron subjected to an external potential to form a semiconductor quantum well wire of cylindrical ring geometry. Besides, as the device has been developed using a GaAs/$Al_{0.35}Ga_{0.65}As$ matrix (the previous works used a matrix of GaN[18,19]), we can assume that the system has only one conduction band partially filled. We assume a parabolic band for the electron, which is split into a sub-band system due to the confinement, and $T = 0$ K. This model is commonly used in the II–VI and III–V semiconductors when the description is near the center of the Brillouin zone in the reduced zone scheme. Under these dynamical conditions, and since the potential barriers do not imply interband transitions or the complex valence band of the III–V and II–VI semiconductor compounds, the contribution of band mixing is small in the confinement regime, which is assumed in this work and it is consistent with the previous treatments.[20,21]

Because of its precision, Raman scattering is a useful technique for studying the electronic structure of nanostructures by considering different polarizations of incident and emitted radiations.[21–23] The analysis of the DCS of a Raman scattering process allows us to determine the sub-band structure of a nanostructured system by a direct inspection of the singularity positions in the spectra, considering the selection rules of transitions of the carriers participating in the interaction with the incident and emitted light of different polarizations. In general, the DCS shows singularities related to the intersub-band and intraband transitions, in our case, only the intersub-band transitions are considered. The result depends on the scattering configurations, and the structure of singularity depends on the incident or emitted photon polarization. The electron Raman scattering has been studied from a theoretical point of view in various systems,

†Corresponding author. E-mail: rbriera@gmail.com
© 2015 Chinese Physical Society and IOP Publishing Ltd

such as quantum well, quantum wire (cross-section with cylindrical disk geometry and also with square geometry), and quantum dot systems. These studies considered the interband and intrasub-band transitions with and without the participation of confinement phonons, also in the presence and absence of external electric and magnetic fields;[24–34] the bulk semiconductor, considering the presence of electric and magnetic fields, was studied too.[35–37] Surface enhanced Raman scattering is one of the most powerful probing methods, which is non-destructive, real-time, good at highly sensitive characterization.[38,39] Raman scattering studies of phonon modes are of fundamental importance for understanding the structural and optical properties, the surface states can lead to novel magnetic properties.[40,41] In the previous studies, the surface optical phonon mode, which is sensitive to the shell thickness, has been found in core/shell quantum dots and core–shell structured nanoparticles. Recently, it has been proposed to be realized in commonly used semiconductors, which suggests a promising approach to the development of semiconductor electronic devices.[41]

In the present work, we present a model of electron Raman scattering for a semiconductor quantum well wire (QWW) of cylindrical ring geometry. The system can be fabricated with GaAs/$Al_{0.35}Ga_{0.65}As$ by using high-resolution electron-beam lithography techniques. The intersub-band ERS processes can be qualitatively described in the following way: first an electron in the conduction band absorbs a photon of incident radiation of energy $\hbar\omega_{\rm l}$, then the electron emits a photon of secondary radiation of energy $\hbar\omega_{\rm s}$ due to a new intersub-band transition.[42]

2. Model and applied theory

Our problem is to determine the stationary states of an electron in a QWW system of cylindrical ring geometry with internal radius $r_{\rm a}$, external radius $r_{\rm b}$, and length L. The envelope function approximation leads to the solution of the Schrödinger equation. The confinement potential is[43]

$$V_{\rm c}=\begin{cases} V_0, & 0\le r<r_{\rm a},\\ 0, & r_{\rm a}\le r<r_{\rm b},\\ V_0, & r_{\rm b}\le r<\infty. \end{cases}$$

The solution of the Schrödinger equation leads to

$$\Psi(\boldsymbol{r}) = \frac{\exp\left[{\rm i}(m\theta+k_z z)\right]}{\sqrt{2\pi L}}u_0(\boldsymbol{r}) \times\begin{cases} AI_m(\gamma r), & 0\le r<r_{\rm a},\\ A_2J_m(\alpha\rho)+B_2Y_m(\alpha r), & r_{\rm a}\le r<r_{\rm b},\\ BK_m(\gamma r), & r_{\rm b}\le r<\infty, \end{cases} \quad (1)$$

with the electron energy

$$\varepsilon_m(k_z)=\varepsilon_{\rm r}+\frac{\hbar^2}{2\mu_{1(2)}}k_z^2,$$

where

$$\alpha=\sqrt{\frac{2\mu_2}{\hbar^2}\varepsilon_{\rm r}},\quad \gamma=\sqrt{\frac{2\mu_1}{\hbar^2}(V_0-\varepsilon_{\rm r})};$$

$u_0(\boldsymbol{r})$ is the electron Bloch function in the band; J_m and Y_m are the Bessel functions of the first and the second kind of order m; I_m and K_m are the modified Bessel functions of the first and the second kind, here we have used the definitions of Bessel functions according to Abramowitz;[44] and μ_1 (μ_2) is the electron effective mass outside (inside) of the QWW. By considering the continuity of the function Ψ and the current density $(1/\mu)(\partial\Psi/\partial r)$ at the interface, we can calculate the constants. Then

$$A=\left[I_1+I_2+I_3\right]^{-1/2},$$
$$A_2=\frac{\bar{A}}{\bar{C}}A,\quad B_2=-\frac{\bar{B}}{\bar{C}}A,$$
$$B=\frac{J_m(\alpha r_{\rm b})\bar{A}+N_m(\alpha r_{\rm b})\bar{B}}{K_m(\gamma r_{\rm b})\bar{C}}A,$$

where

$$I_1=\int_0^{r_{\rm a}}I_m^2(\gamma r)r\,{\rm d}r,$$
$$I_2=\frac{1}{\bar{C}^2}\int_{r_{\rm a}}^{r_{\rm b}}\left[\bar{A}J_m(\alpha r)-\bar{B}N_m(\alpha r)\right]^2 r\,{\rm d}r,$$
$$I_3=\left[\frac{J_m(\alpha r_{\rm b})\bar{A}+N_m(\alpha r_{\rm b})\bar{B}}{K_m(\gamma r_{\rm b})\bar{C}}\right]^2\int_{r_{\rm b}}^{\infty}K_m^2(\gamma r)r\,{\rm d}r,$$
$$\bar{A}=I_m(\gamma r_{\rm a})N_m'(\alpha r_{\rm a})-\beta I_m'(\gamma r_{\rm a})N_m(\alpha r_{\rm a}),$$
$$\bar{B}=I_m(\gamma r_{\rm a})J_m'(\alpha r_{\rm a})-\beta I_m'(\gamma r_{\rm a})J_m(\alpha r_{\rm a}),$$
$$\bar{C}=J_m(\alpha r_{\rm a})N_m'(\alpha r_{\rm a})-J_m'(\alpha r_{\rm a})N_m(\alpha r_{\rm a}),$$

with $\beta=\sqrt{(\mu_1/\mu_2)(V_0-\varepsilon_{\rm r})/\varepsilon_{\rm r}}$ and $\varepsilon_{\rm r}$ being determined from the following transcendental equation:

$$\bar{A}\left[K_m(\gamma r_{\rm b})J_m'(\gamma r_{\rm b})-\beta K_m'(\gamma r_{\rm b})J_m(\gamma r_{\rm b})\right] = \bar{B}\left[K_m(\gamma r_{\rm b})N_m'(\gamma r_{\rm b})-\beta K_m'(\gamma r_{\rm b})N_m(\gamma r_{\rm b})\right]. \quad (2)$$

As can be observed, for each value of m, n energy values are obtained. The states are then described by the following quantum numbers: $m=0,1,\ldots$; $n=1,2,\ldots$; and k_z (see Refs. [32] and [42]).

3. Raman cross-section

The Raman differential cross-section in a volume per unit solid angle for incoming light of frequency $\omega_{\rm l}$ and scattered light of frequency $\omega_{\rm s}$ is given in Refs. [24] and [25], and it can be written as

$$\frac{{\rm d}^2\sigma}{{\rm d}\omega_{\rm s}\,{\rm d}\Omega}=\frac{V^2\omega_{\rm s}^2\eta(\omega_{\rm s})}{8\pi^3c^4\eta(\omega_{\rm l})}W(\omega_{\rm l},e_{\rm l},\omega_{\rm s},e_{\rm s}), \quad (3)$$

where $\eta(\omega_\rho)$ is the refraction index as a function of the radiation with frequency ω_ρ; e_ρ is the light polarization unit vector; the subindex $\rho=l$ (s) indicates the incident (secondary) radiation; c is the light velocity in a vacuum, and $W(\omega_{\rm l},e_{\rm l},\omega_{\rm s},e_{\rm s})$

is the transition rate for the absorption and emission radiation calculated according to Fermi's golden rule

$$W(\omega_{\rm l},\boldsymbol{e}_{\rm l},\omega_{\rm s},\boldsymbol{e}_{\rm s})=\frac{2\pi}{\hbar}\sum_f|M_f|^2\delta(E_f-E_i), \tag{4}$$

with

$$M_f=\sum_a\frac{\langle f|\hat{H}_{\rm s}|a\rangle\langle a|\hat{H}_{\rm l}|i\rangle}{E_i-E_a+{\rm i}\Gamma_a}+\sum_b\frac{\langle f|\hat{H}_{\rm l}|b\rangle\langle b|\hat{H}_{\rm s}|i\rangle}{E_i-E_b+{\rm i}\Gamma_b}. \tag{5}$$

Here $\hat{H}_\rho$ is the Hamiltonian operator for the radiation field, in the dipole approximation, with frequency ω_ρ and polarization unit vector $\boldsymbol{e}_\rho$,[42] while $|i\rangle$ and $|f\rangle$ are the initial and the final states with energies E_i and E_f, respectively; and $|a\rangle$ and $|b\rangle$ are the intermediate states with energies E_a and E_b, whose lifetimes are Γ_a and Γ_b. In this case, we have two possibilities:[42] (i) the electron absorbs the incident photon and later emits the secondary radiation photon, which is represented by the first term of Eq. (5); (ii) the electron emits the secondary radiation photon and later absorbs the incident photon which is represented by the second term of Eq. (5).

The Hamiltonian operator for the radiation field has the form

$$\hat{H}_\rho=\sqrt{\frac{2\pi\hbar e^2}{V\omega_\rho}}\frac{(\hat{\boldsymbol{e}}_\rho\cdot\hat{\boldsymbol{p}})}{\mu}, \tag{6}$$

where $\hat{\boldsymbol{p}}=-{\rm i}\hbar\boldsymbol{\nabla}$ and μ is the electron effective mass.

The dipole approximation is commonly used in studying electron Raman scattering and resonant Raman scattering in nanostructures. This approximation is valid as long as the radiation wavelength is much longer than the radius of the wire. The effect of reduced dimensionality on the free carrier absorption and the selection rules for intersub-band transition has been discussed in Ref. [42], and there it is shown that the ERS can only take place in the confinement direction, then

$$\hat{\boldsymbol{p}}=-{\rm i}\hbar(\boldsymbol{\nabla}_+\boldsymbol{e}_-+\nabla_-\boldsymbol{e}_+),$$

where

$$\nabla_\pm=\frac{\exp(\pm{\rm i}\theta)}{\sqrt{2}}\left[\frac{\partial}{\partial r}\pm\frac{\rm i}{r}\frac{\partial}{\partial\theta}\right],\quad \boldsymbol{e}_\pm=\frac{\boldsymbol{e}_x\pm{\rm i}\boldsymbol{e}_y}{\sqrt{2}}.$$

Now we must calculate the matrix elements appearing in Eq. (4). We use the condition $\boldsymbol{k}=\boldsymbol{0}$ for the radiation field;[24,42] thus, by considering Eqs. (1) and (6), the following matrix elements are obtained:

$$\begin{aligned}&\langle\Psi_{m',n',k_z'}|\hat{H}_\rho|\Psi_{m'',n'',k_z''}\rangle_\pm\\&=-{\rm i}\hbar\frac{|e|}{\mu_0(r_{\rm b}-r_{\rm a})}\sqrt{\frac{2\pi\hbar}{V\omega_\rho}}(\boldsymbol{e}_\rho\cdot\boldsymbol{e}_\pm)T_\pm(m',m'')\\&\times\delta_{m'\pm1,m''}\delta_{k_z',k_z''},\end{aligned} \tag{7}$$

where $\Psi_{m',n',k_z'}$ and $\Psi_{m'',n'',k_z''}$ are the final and the initial states of the transition, respectively,

$$T_\pm(m',m'')={\rm I}_{m'm''}\mp m''{\rm II}_{m'm''},$$

and μ_0 is the electron free mass. The explicit forms of ${\rm I}_{m'm''}$ and ${\rm II}_{m'm''}$ are very complicated and their expressions can be calculated following the method reported in Ref. [42]. As can be observed, the emission or absorption of one photon can only take place between consecutive states of the quantum number$m$ according to the selection rule $m''=m'\pm1$, while there is no restriction on quantum number n (see Eq. (7)).

In the initial state, we have an electron in a conduction subband and an incident radiation photon; and for the final state, we have an electron in the other conduction subband and a secondary radiation photon;

$$E_i=\hbar\omega_{\rm l}+\varepsilon_{m'',n''}(k_z),\quad E_f=\hbar\omega_{\rm s}+\varepsilon_{m,n}(k_z). \tag{8}$$

For the intermediate states,

$$E_a=\varepsilon_{m',n'}(k_z),\quad E_b=\hbar\omega_{\rm l}+\hbar\omega_{\rm s}+\varepsilon_{m',n'}(k_z). \tag{9}$$

Using Eqs. (3)–(9), we obtain four different contributions to the differential cross section depending on the polarizations of the incident and the emitted radiations, finally we can write Eq. (3) as

$$\begin{aligned}\left[\frac{{\rm d}^2\sigma}{{\rm d}\omega_{\rm s}{\rm d}\omega}\right]&=\left[\frac{{\rm d}^2\sigma}{{\rm d}\omega_{\rm s}{\rm d}\omega}\right]_{++}+\left[\frac{{\rm d}^2\sigma}{{\rm d}\omega_{\rm s}{\rm d}\omega}\right]_{+-}\\&+\left[\frac{{\rm d}^2\sigma}{{\rm d}\omega_{\rm s}{\rm d}\omega}\right]_{-+}+\left[\frac{{\rm d}^2\sigma}{{\rm d}\omega_{\rm s}{\rm d}\omega}\right]_{--},\end{aligned}$$

where

$$\begin{aligned}&\left[\frac{{\rm d}^2\sigma}{{\rm d}\omega_{\rm s}{\rm d}\omega}\right]_{\pm\pm}\\&=\frac{\eta(\omega_{\rm s})}{\eta(\omega_{\rm l})}\left(\frac{e}{c}\right)^4\frac{\hbar\Gamma_f}{\pi d\mu_0^2}\frac{\omega_{\rm s}}{\omega_{\rm l}}(\sigma_{\rm s}^{\pm}\cdot\sigma_{\rm l}^{\pm})^2\\&\times\sum_{m,n,n''}\frac{|M_{\pm\pm}|^2}{[\hbar\omega_{\rm l}-\hbar\omega_{\rm s}+\varepsilon_{\rm r}(m+2,n'')-\varepsilon_{\rm r}(m,n)]^2+\Gamma_f^2},\\&\left[\frac{{\rm d}^2\sigma}{{\rm d}\omega_{\rm s}{\rm d}\omega}\right]_{\pm\mp}\\&=\frac{\eta(\omega_{\rm s})}{\eta(\omega_{\rm l})}\left(\frac{e}{c}\right)^4\frac{\hbar\Gamma_f}{\pi d\mu_0^2}\frac{\omega_{\rm s}}{\omega_{\rm l}}(\sigma_{\rm s}^{\pm}\cdot\sigma_{\rm l}^{\mp})^2\\&\times\sum_{m,n,n''}\frac{|M_{\pm\mp}|^2}{[\hbar\omega_{\rm l}-\hbar\omega_{\rm s}+\varepsilon_{\rm r}(m,n'')-\varepsilon_{\rm r}(m,n)]^2+\Gamma_f^2},\end{aligned}$$

$$\begin{aligned}M_{\pm\pm}&=\frac{\hbar^2}{2\mu_0d^2}\sum_{n'}T_\pm(m,m\pm1)T_\pm(m+1,m\pm2)\\&\times\left[\frac{1}{\hbar\omega_{\rm s}+\varepsilon_{\rm r}(m,n)-\varepsilon_{\rm r}(m\pm1,n')+{\rm i}\Gamma_a}\right.\\&\left.-\frac{1}{\hbar\omega_{\rm l}-\varepsilon_{\rm r}(m,n)+\varepsilon_{\rm r}(m\pm1,n')-{\rm i}\Gamma_b}\right],\end{aligned} \tag{10}$$

$$M_{\pm\mp} = \frac{\hbar^2}{2\mu_0 d^2}\sum_{n'} T_{\pm}(m,m\pm1)T_{\pm}(m+1,m) \times \left[\frac{1}{\hbar\omega_{\rm s}+\varepsilon_{\rm r}(m,n)-\varepsilon_{\rm r}(m\pm1,n')+{\rm i}\Gamma_a} - \frac{1}{\hbar\omega_{\rm l}-\varepsilon_{\rm r}(m,n)+\varepsilon_{\rm r}(m\pm1,n')-{\rm i}\Gamma_b}\right], \quad (11)$$

$$\sigma_\rho^{\pm} = \boldsymbol{e}_\rho \cdot \boldsymbol{e}_{\pm}, \quad d = r_{\rm b} - r_{\rm a}.$$

4. Calculation of Raman scattering intensities

Consider first the behaviors of the electronic states for a semiconductor quantum well/shell of cylindrical geometry formed in a matrix of GaAs/$Al_{0.35}Ga_{0.65}As$, the parameters needed are $\mu_1 = 0.0665\mu_0$, $\mu_2 = 0.096\mu_0$, and $V_0 = 0.30$ eV,[43] where μ_0 is the free electron mass. Figure 1(a) shows the energies corresponding to the system with $r_{\rm b} = 100$ Å. The straight lines represent the energies of a quantum wire with a radius of 100 Å, obtained using Eq. (2). It can be seen that increasing $r_{\rm a}$ causes an increase in energy for all the different states of the QWW due to the fact that we increase the confinement of the electrons. It is also visible that these increases in energy are not the same for all levels. The increase of $r_{\rm a}$ means the increase of the confinement, and it can remove all levels within the QWW. This effect is modulated by the barrier height of the system. From Figs. 1(a) and 1(b), it can be concluded that the states are grouped into several sub-bands; these sub-bands are determined by the quantum number n. When n is larger, the energies of the states that make up the sub-band are bigger. Within each sub-band, there are levels with quantum number m, and the energy increases with increasing m. As can be seen in Fig. 1(a), the energy of the state with $m = 0$ and $n = 1$ is almost constant up to $r_{\rm a} = 4$ Å, the remaining values are similar to those of a quantum wire with $r_{\rm a} = 0$ Å and $r_{\rm b} = 100$ Å; while the energy of the state with $m = 1$ and $n = 1$ is almost constant up to $r_{\rm a} = 15$ Å, and the energy of the state with $m = 2$ and $n = 1$ is almost constant up to $r_{\rm a} = 25$ Å. This means that the effect of the confinement on the quantum state decreases with increasing energy and quantum number m in each sub-band (see Fig. 1(b)). In Fig. 1(b), we increase the radius to $r_{\rm b} = 200$ Å. As shown in this figure, this increase causes the states to significantly reduce their energy, with a greater reduction for states with higher quantum numbers m and n. Also, in this case, it is seen that increasing $r_{\rm b}$ involves increasing the number of states "within" the system. Furthermore, crosses are observed between the levels of different sub-bands, but not between levels of the same sub-band.

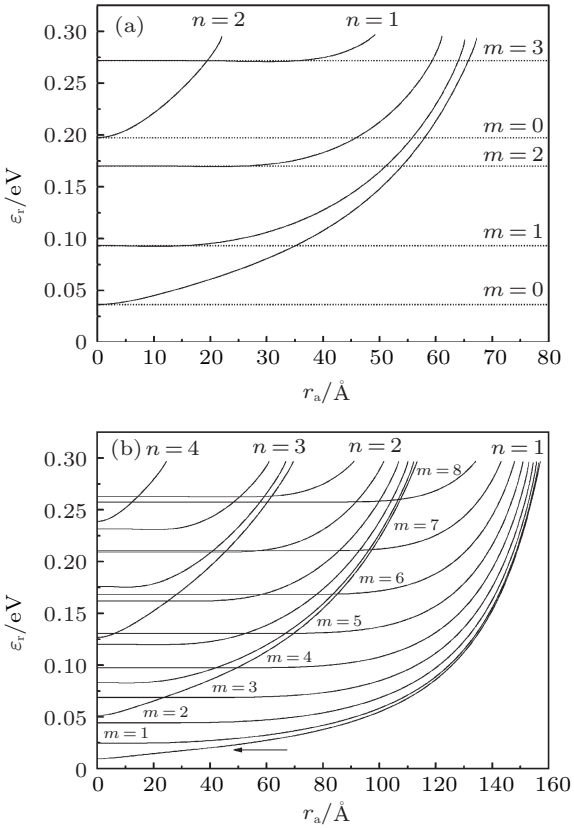


Fig. 1. Electron energies $\varepsilon_{\rm r}$ corresponding to a semiconductor quantum well wire with (a) $r_{\rm b} = 100$ Å, (b) $r_{\rm b} = 200$ Å. The dotted line in panel (a) corresponds to the energy of a quantum well wire with $r_{\rm a} = 0$ Å and $r_{\rm b} = 100$ Å.

In Fig. 2, we study QWW of various widths (a) $d = 80$ Å, (b) $d = 100$ Å; where the solid and dashed lines correspond to the states with $n = 1$ and $n = 2$, respectively. As can be observed, the states are grouped into sub-bands, again determined by the quantum number n. It can be observed that increasing the width increases the number of energy levels within the QWW. Moreover, increasing $r_{\rm a}$ leads to more energy levels in the well because the QWW system volume increases. In the case that $r_{\rm a}$ is approximately 300 Å, it does not reproduce the energy values corresponding to a quantum well of width d because even for these radii, the cylindrical symmetry is preserved. Furthermore, it is interesting to note that the states tend to minimal energy for each n. This is due to the fact that QWW always has a fixed width, so for $r_{\rm a} \to \infty$ it should reproduce the energy values corresponding to a quantum well with width d.[43]

Equations (10) and (11) have resonant singularities which are independent of the incident photon or the secondary photon when

$$\hbar\omega_\rho(m\pm1,,n',m,n) \to \hbar\omega_\rho = \varepsilon_{\rm r}(m\pm1,n') - \varepsilon_{\rm r}(m,n),$$

and non-resonant singularities which are dependent on the incident photon or the secondary photon when

$$\hbar\omega_\rho(m+a,n'',m,n) \to \hbar\omega_\rho$$

$$= \begin{cases} \hbar\omega_{\rm s} - \varepsilon_{\rm r}(m+a,n'') + \varepsilon_{\rm r}(m,n), & \rho = {\rm l}, \\ \hbar\omega_{\rm l} + \varepsilon_{\rm r}(m+a,n'') - \varepsilon_{\rm r}(m,n), & \rho = {\rm s}, \end{cases}$$

where $a = 2$ for $(\sigma_{\rm s}^+, \sigma_{\rm l}^+)$ and $(\sigma_{\rm s}^-, \sigma_{\rm l}^-)$ polarizations, and $a = 0$ for $(\sigma_{\rm s}^+, \sigma_{\rm l}^-)$ and $(\sigma_{\rm s}^-, \sigma_{\rm l}^+)$ polarizations.

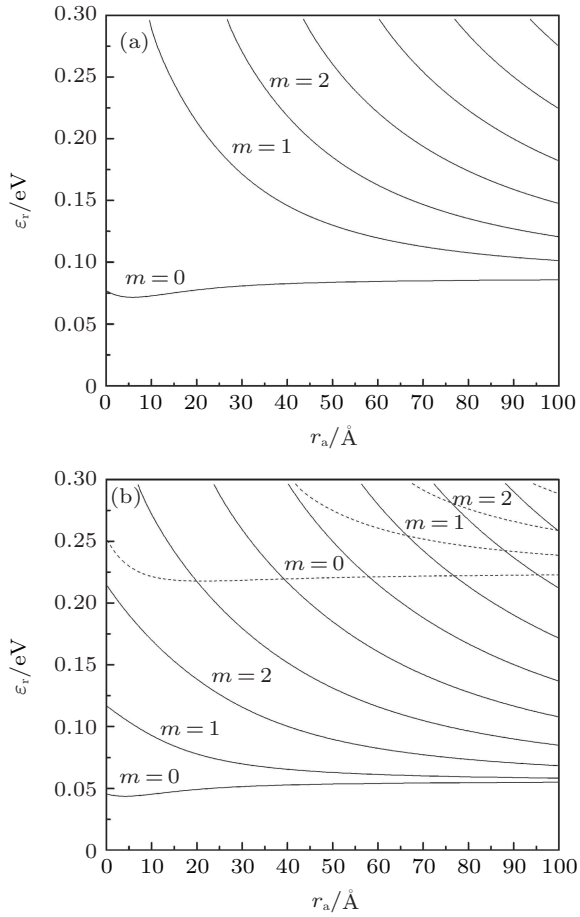


Fig. 2. The electron energies $\varepsilon_{\rm r}$ corresponding to a semiconductor quantum well wire with (a) $d = 80$ Å, (b) $d = 100$ Å. The solid line corresponds to $n = 1$ electron states, and the dotted line corresponds to $n = 2$ electron states.

In general, the system behavior is very similar to that described in Ref. [42], considering that $B = 0$ T; however, some differences are detailed below. Figure 3(a) shows the differential cross section for the polarizations $(\sigma_{\rm s}^+, \sigma_{\rm l}^+)$ for $\hbar\omega_{\rm l} = 0.28$ eV by changing the inner radius of the system, $r_{\rm a}$. As noted, the increase of the inner radius causes the displacement of the resonant singularities at lower energy setting. This is because the gap between the energy levels decreases when increasing the confinement (see Fig. 1). In Fig. 3(b), we have a configuration similar to that of Fig. 4(a), but it has increased outer radius $r_{\rm b}$. This causes the displacement of the resonant singularities to lower values of energy because if the outer radius is larger, the number of electron states within the quantum wire is larger, thus reducing the gap between the energy levels which also causes a reduction in the intensity of the singularity. Furthermore, it is observed that the increase of $r_{\rm a}$ changes the intensity of the singularity, showing that there is an optimal inner radius for each value of outer radius. In Fig. 4, we can see that with increasing medium radius, $(r_{\rm a} + r_{\rm b})/2$, while the width of the wire, d, remains constant, the resonant singularities are shifted to lower energy values (see Fig. 2), the graph changes into a pattern similar to those shown in Figs. 3(a) and 3(b). In this case, there is also an optimal medium radius for each wire width.

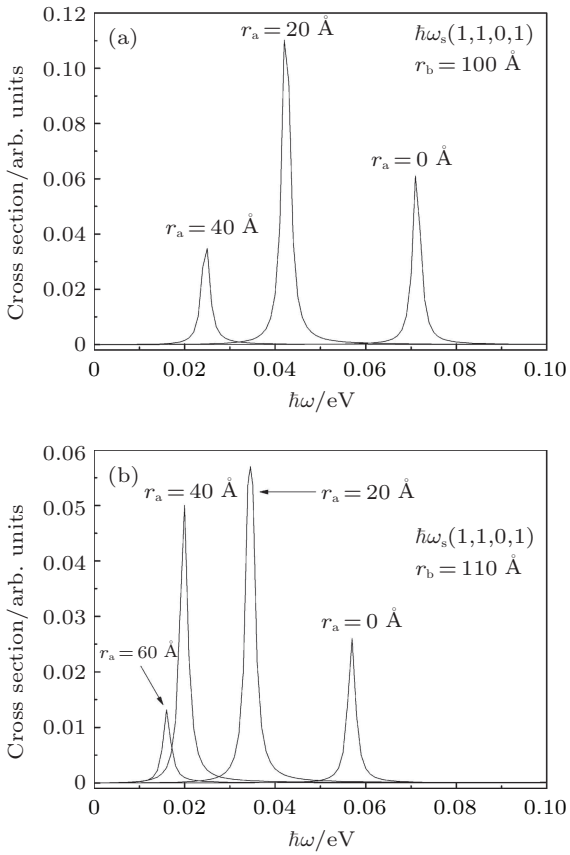


Fig. 3. Differential cross section for a semiconductor quantum well wire with $(\sigma_{\rm s}^+, \sigma_{\rm l}^+)$ polarization, where $\hbar\omega_{\rm l} = 0.28$ eV; (a) $r_{\rm b} = 100$ Å, (b) $r_{\rm b} = 110$ Å.

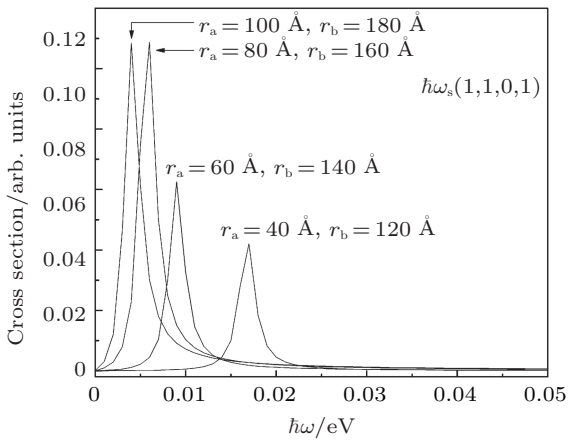


Fig. 4. Differential cross sections for a semiconductor quantum well wire with $(\sigma_{\rm s}^+, \sigma_{\rm l}^+)$ polarization, where $\hbar\omega_{\rm l} = 0.28$ eV and $d = 80$ Å.

5. Conclusion

We present the formulas for calculating the electron Raman scattering intensities for the semiconductor quantum

well wire with a cylindrical ring cross-section grown in a GaAs/$Al_{0.35}Ga_{0.65}As$ matrix. Furthermore, we demonstrate that the structure of the differential cross-section as given in figures, provides a transparent understanding of the energy sub-band structure. The results presented in this work are similar to those previously obtained in other theoretical work.[42] Moreover, we show that any change in the system configuration leads to changes in the intensity and the frequency of the secondary radiation. This effectively shows that Raman spectroscopy is a powerful probe for semiconductor nanostructures due to the material-selective resonant enhancement. In addition, we note that in this work we have applied a simplified model for the electron structure of the system. In a more realistic case, we should consider a coupled band structure by using models like the Luttinger–Kohn or the Kane model. The Raman scattering process considering the electron–phonon interaction is studied using the dielectric continuum approach which has separate sets of confined and surface (interface) modes.

References

[1] Zhoo X F and Liu C H 2007 *Phys. Lett. A* **364** 70
[2] Zhoo X F and Liu C H 2006 *Eur. Phys. J. B* **53** 209
[3] Liu Y, Liang P, Shu H B, Cao D, Dong Q M and Wang L 2014 *Chin. Phys. B* **23** 067304
[4] Xu Z H, Xiao W and Chen Y G 2013 *Chin. Phys. Lett.* **30** 057201
[5] Milekhin A G, Toropov A I, Bakarov A K, Schulze S and Zahn D R T 2006 *JETP Lett.* **83** 505
[6] Milekhin A G, Nikiforov A I, Pchelyakov O P and Pisma Zh. Éksp 2005 *Teor. Fiz.* **81** 33
[7] Milekhin A G, Tenne D A and Zahn D R T 2003 *Quantum Dot Structures: Raman and Infrared Spectroscopy, Quantum Dots and Nanowires* (Stevenson Ranch: American Scientific Publishers) p. 375
[8] Tenne A D, Bakarov A K, Toropov A I and Zahn D R T 2002 *Physica E* **13** 199
[9] Liang Y, Zhai L, Zhao X and Xu D 2005 *J. Phys. Chem. B* **109** 7120
[10] Liu W, Liu S L, Chen D N and Niu H B 2014 *Chin. Phys. B* **23** 104202
[11] Peng Z L, Liang S and Deng L G 2009 *Chin. Phys. Lett.* **26** 127301
[12] Chou M H, Liu S B, Huang C Y, Wu S Y and Cheng C L 2008 *Appl. Surf. Sci.* **254** 7539
[13] Sood A K, Menéndez J, Cardona M and Ploog K 1985 *Phys. Rev. Lett.* **54** 2115
[14] Zhong Q H and Yi X H 2010 *Superlatt. Microstruct.* **47** 723
[15] Zhong Q H and Sun Y T 2011 *Thin Solid Films* **519** 8178
[16] Wang J, Demangeot F, Pechou R, Ponchet A, Cros A and Daudin B 2012 *Phys. Rev. B* **85** 155432
[17] Livneh T, Zhang J P, Cheng G S and Moskovits M 2006 *Phys. Rev. B* **74** 035320
[18] Laneuville V, Demangeot F, Pchou R, Salles P, Ponchet A, Jacopin G, Rigutti L, de Luna Bugallo A, Tchernycheva M, Julien F H, March K, Zagonel L F and Songmuang R 2011 *Phys. Rev. B* **83** 115417
[19] Liu H L, Chen C C, Chia C, Yeh C C, Chen C H, Yu M Y, Keller S and DenBaars S P 2001 *Chem. Phys. Lett.* **345** 245
[20] Betancourt-Riera R, Rosas R, Marín-Enriquez I, Riera R and Marin J L 2005 *J. Phys.: Condens. Matter* **17** 4451
[21] Betancourt-Riera R, Riera R, Marín J L and Rosas R A 2004 *Electron Raman Scattering in Nanostructures, Encyclopedia of Nanoscience and Nanotechnology* (Stevenson Ranch: American Scientific Publishers) Vol. 3 p. 101
[22] Kushwaha M S 2001 *Surf. Sci. Rep.* **41** 1
[23] Riera R, Marín J L and Rosas R A 2001 *Optical Properties and Impurity States in Nanostructured Materials, Handbook of Advanced Electronic and Photonic Devices* (New York: Academic) Vol. 6 chapter 6
[24] Betancourt-Riera R, Betancourt-Riera R, Nieto J J M and Riera R 2013 *Physica B* **410** 126
[25] Betancourt-Riera R, Betancourt-Riera R, Rosas R and Riera R 2012 *J. Comput. Theor. Nanosci.* **9** 1
[26] Lu F, Liu C H and Guo Z L 2012 *Physica B* **407** 165
[27] Zhai L X, Wang Y and Liu J J 2011 *J. Appl. Phys.* **110** 043701
[28] Zhong Q H and Yi X H 2010 *Superlattices and Microstructures* **47** 723
[29] Zhong Q H, Liu C H, Zhang Y Q and Sun H C 2008 *Phys. Lett. A* **372** 2103
[30] Scheinert M, Sigg H and Tsujino S 2007 *Appl. Phys. Lett.* **91** 131108
[31] Ismailov T G and Mehdiyev B H 2006 *Physica E* **31** 72
[32] Bergues J M, Betancourt-Riera R, Riera R and Marin J L 2000 *J. Phys.: Condens. Matter* **12** 7983
[33] Bergues J M, Betancourt-Riera R, Marin J L and Riera R 1996 *Phys. Low-Dimens. Struct.* **7/8** 81
[34] Riera R, Comas F, Trallero-Giner C and Pavlov S T 1988 *Phys. Status Solid B* **148** 533
[35] Comas F, Trallero Giner C and Perez-Alvarez R 1986 *J. Phys. C: Solid State Phys.* **19** 6479
[36] Trallero-Giner C, Ruf T and Cardona M 1990 *Phys. Rev. B* **41** 3028
[37] González de la Cruz G and Trallero-Giner C 1998 *Phys. Rev. B* **58** 9104
[38] Wang M L, Zhang C X, Wu Z L, Jing X L and Xu H J 2014 *Chin. Phys. B* **23** 067802
[39] Jiang S M, Wu D J, Wu X W and Liu X J 2014 *Chin. Phys. B* **23** 047807
[40] Wang M, Tian Y, Zhang J M, Guo C F, Zhang X Z and Liu Q 2014 *Chin. Phys. B* **23** 087803
[41] Shi L K and Lou W K 2014 *Chin. Phys. Lett.* **31** 067304
[42] Betancourt-Riera R, Nieto Jalil J M, Riera R, Betancourt-Riera R and Rosas R 2008 *J. Phys.: Condens. Matter* **20** 045203
[43] Betancourt-Riera R, Betancourt-Riera R, Jordán Hernández R and Riera R 2012 *Revista Electrónica Nova Scientia* **9** 89
[44] Abramowitz M and Stegun I A 1972 *Handbook of Mathematical Functions with Formulas, Graphs, and Mathematical Tables* (New York: Dover Publications)